




Synthesis and fluorescence sensing of energetic materials using benzenesulfonic acid-doped polyaniline

Satish A. Ture^{1,2}, Shruthy D. Pattathil², Veerabhadragouda B. Patil^{2,3}, Channabasaveshwar V. Yelamaggad⁴, Ramón Martínez-Máñez^{5,6}, and Venkataraman Abbaraju^{1,2,7,8,*} 

¹Department of Chemistry, Gulbarga University, Kalaburagi, Karnataka 585106, India

²Materials Chemistry Laboratory, Department of Materials Science, Gulbarga University, Kalaburagi, Karnataka 585106, India

³Institute of Energetic Materials, Faculty of Chemical Technology, University of Pardubice, Studentska 92, 53210 Pardubice, Czech Republic

⁴Centre for Nano and Soft Matter Sciences (CeNS), Bengaluru, Karnataka 560013, India

⁵Instituto Interuniversitario de Investigación de Reconocimiento Molecular y Desarrollo Tecnológico (IDM), Universitat Politècnica de València, Universitat de València, Camino de Vera s/n, 46022 Valencia, Spain

⁶CIBER de Bioingeniería, Biomateriales y Nanomedicina (CIBER-BBN), Madrid, Spain

⁷Khaja Bandanawaz University, Kalaburagi, Karnataka 585104, India

⁸R&D centre, Premier Explosives Limited, Peddakandukur, Telangana 508286, India

Received: 2 April 2021

Accepted: 29 June 2021

Published online:

9 July 2021

© The Author(s), under exclusive licence to Springer Science+Business Media, LLC, part of Springer Nature 2021

ABSTRACT

The Fluorescence sensing technique for trace detection of High Energy Materials (HEMs) has gained more attention in recent times. In the present paper, the interaction between the fluorophore and HEMs is studied using spectroscopic and electrochemical techniques. The fluorophore polyaniline (PANI) was functionalised by doping it with benzenesulfonic acid (BSA) to increase the processability, and mobility of π -electrons along with decreased π -stacking. It is observed that upon doping the solubility of BSA-PANI is increased, facilitating a higher quenching by commercial explosives, i.e., RDX, CL-20, CL-20:RDX cocrystal. The interaction studies undertaken through fluorescence quenching, FTIR and Resonance Raman studies shows that the benzenoid unit, polaron and bipolaron nitrogen in BSA-PANI interact with nitro groups of HEMs and form a charge-transfer complex between HEMs and BSA-PANI undergoing predominantly a PET mechanism. LOD value is found to be least for Cocrystal (1.876×10^{-5} M) when compared to other HEMs 3.191×10^{-5} M (CL-20), 5.904×10^{-5} M (RDX), 3.734×10^{-5} M (PETN) indicating that cocrystal can be detected in trace level. The collaborative study between cyclic voltammetry and

Address correspondence to E-mail: raman.dms@gmail.com

the observed results of fluorescence quenching, revealed that the emeraldine salt form of (BSA-PANI) is sensitive to HEMs.

1 Introduction

The development of sensors for quick and sensitive detection of HEMs [PA (Picric acid), RDX (1,3,5-trinitroperhydro-1,3,5-triazine), PETN (pentaerythritol tetranitrate), CL-20 (hexanitrohexaazaisowurtzitan), etc.] has garnered more interest in recent years [1]. HEMs are mostly fabricated for use in military and commercial purposes. The degradation products and by-products of HEMs cause an adverse effect on the environment, especially soil and water where there stored and produced [2]. In recent years, the use of HEMs by terrorist groups has increased; therefore, their detection in the solid, liquid, or vapour phase is of utmost importance for the safety of the citizens. The techniques such as Raman spectra, ion mobility spectroscopy, mass spectroscopy, chromatography and electrochemical technique are used for the detection of HEMs [3, 4]. The fluorescence technique is the most sensitive technique to detect HEMs with high selectivity, low cost, and ease to handle. In this technique, fluorophore acts as an electron donor and the analyte HEMs acts as an acceptor. In the literature, fluorescence quenching (turn off) and enhancing (turn on) mechanisms for the detection of HEMs are reported. Swager et al. [5] in 1998 used fluorescence turn-on mechanism for the detection of explosives using an exotic conducting polymer pentiptycene polymer and the other conjugated polymers such as polyacetylenes, poly(p-phenylenevinyls) etc., were reported for the detection of TNT using fluorescence turn-on mechanism [6, 7]. Heran Nie et al. used conjugated copolymer film as electroactive material for the detection of TNT in an aqueous medium [8]. Paul Martinez et al. synthesised luminescent organosilicon copolymers poly(silafluorenyldiethynylspirobifluorene) and poly(tetrasilolethynylspirobifluorene) for detection of explosive mixture such as TNT, DNT, PA, HMX, RDX, CL-20 using fluorescence quenching technique along with separation by employing chromatographic support [9].

In the literature, there are reports on fluorogenic chemosensors used for the detection of anions. These anions quench the fluorescence emission through a

non-radiative pathway [10–12]. Our group has earlier reported work on doped polyaniline for the detection of nitroaromatics, like picric acid, p-nitrotoluene etc., indicating that doped polyaniline is capable of studying other complex HEMs [13, 14]. Our present work reveals that detection of HEMs using doped polyaniline with other complex HEMs such as RDX, PETN, CL-20 and CL-20: RDX Cocrystal shown in Scheme 1. The sensing of these HEMs is essential because RDX is most commonly used in terrorist attacks and commercial explosives. PETN is primarily used in detonators and landmines [15]. CL-20 is the most powerful green energetic material compared to RDX and TNT [16]. Whereas CL-20: RDX Cocrystals are the next generation energetic materials with improved characteristics without affecting the energy of its sub crystals [17]. The doped polyaniline is a conjugated polymer that acts as a fluorophore and show a molecular wire effect during fluorescence quenching studies. The doping process in polyaniline increases solubility and processability with decreased π stacking between polymer chains. Upon doping the polymer chain with suitable dopant the conductivity of the polymer chain enhances [18]. The emeraldine salt form with benzenoid, quinoid, polaron and bipolaron units in the polymer are sensitive towards the interaction with the HEMs [13].

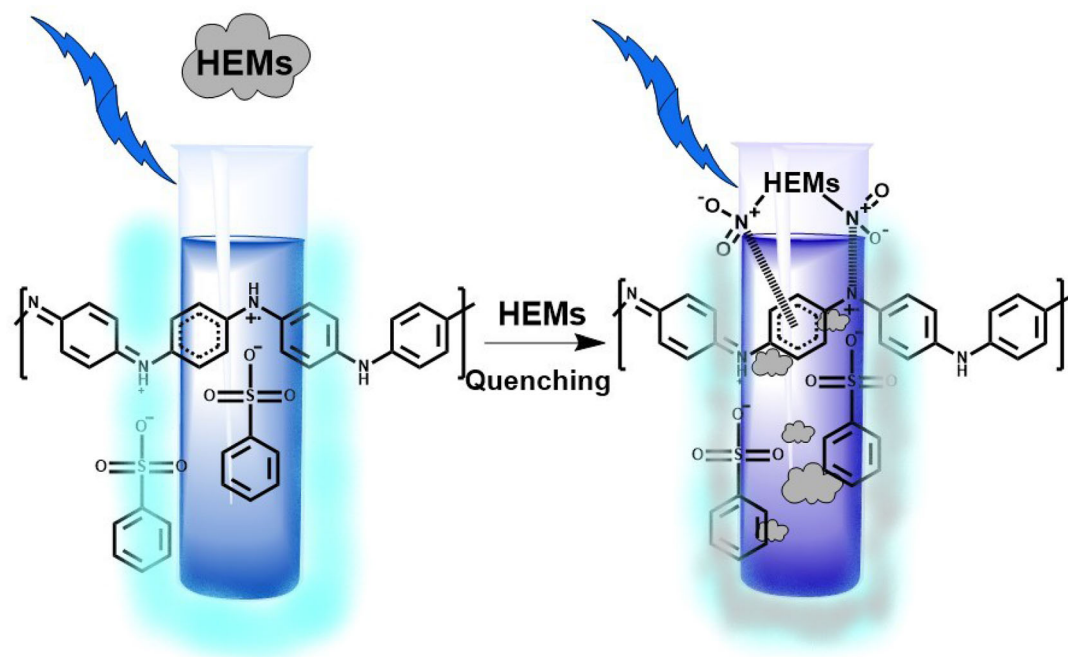
In the present study, BSA-doped PANI is synthesised and used as a fluorophore. In this paper, we have undertaken a detailed study and explained details of characterisation techniques (UV-Vis, FTIR, Raman spectroscopy). The details on the interaction mechanism taking place during fluorescence quenching are explained based on spectroscopic techniques Viz. FTIR, Resonance Raman spectra, and electrochemical studies.

2 Experiment

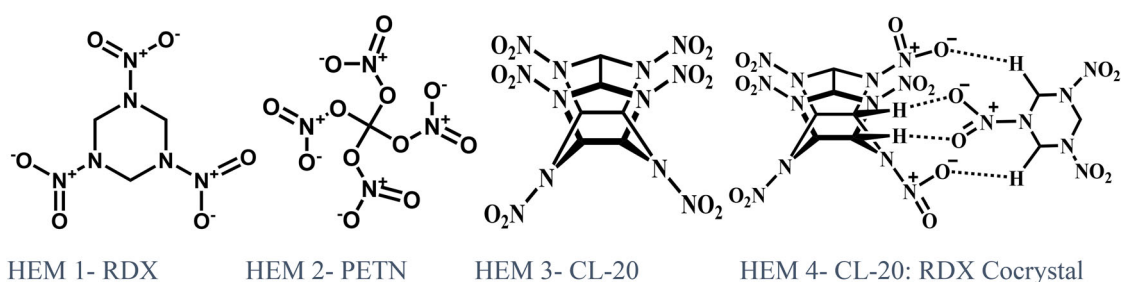
2.1 Materials and methods

Aniline, ammonium per-sulfate (APS), benzenesulfonic acid (BSA), and other solvents were of analytical grade. RDX, CL-20, PETN was provided in

$$\lambda_{\text{ex}} = 352\text{nm} \quad \lambda_{\text{em}} = 435\text{nm}$$



BSA doped Polyaniline BSA doped Polyaniline with HEMs



Scheme 1 BSA-doped polyaniline and interaction of HEMs with BSA-doped Polyaniline

anhydrate form with 99% purity by Premier Explosives Limited, Hyderabad, India. CL-20: RDX cocrystal was synthesised by a solvent evaporation method using acetone as solvent [17].

2.2 Synthesis of BSA-doped polyaniline

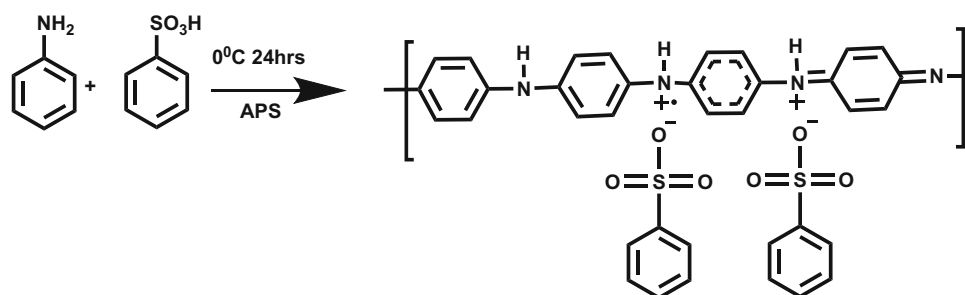
The benzenesulfonic acid-doped polyaniline (BSA-PANI) was synthesised by chemical oxidative polymerization as reported by MacDiarmid et al. [14, 19] and shown in Scheme 2. The synthesis involves preparing an equimolar mixture of aniline and benzenesulfonic acid (BSA). A precooled solution of APS

acting as an oxidizer was added dropwise to this mixture at 0–5 °C. After complete addition, the reaction mixture was stirred for 24 h to complete the polymerization in cold conditions. Then, the solution is filtered, washed with water/methanol and dried at 60 °C for 12 h to get a dark green powder of BSA-PANI.

2.3 Characterisation

BSA-PANI and BSA-PANI on interaction with HEMs were characterised by FT-IR, Resonance Raman, UV–Vis, Fluorescence spectroscopy and Cyclic

Scheme 2 Schematic model for the synthesis of BSA-PANI



voltammetry. The morphology of BSA-PANI and BSA-PANI on interaction with HEMs samples were investigated by FESEM. The solid samples for FT-IR, Resonance Raman and FESEM studies were prepared by dissolving HEMs in acetone and added to BSA-PANI followed by evaporation, drying and then taken for analysis. The FTIR analysis was carried out using Perkin Elmer IR spectrometer 1000 using KBr pellet method in the range of 400 cm^{-1} to 4000 cm^{-1} . The Resonance Raman spectra were recorded by Horiba Jobin Yvon instrument within the range of 60 cm^{-1} to 2500 cm^{-1} employing laser wavelengths of 638 nm with laser power of 25% of 25 mW. The absorption spectra were analysed using UV-Vis spectrometer PG Instruments Limited T90+ ranging from 200 to 900 nm. The fluorescence quenching studies were carried by Horiba Jobin Yvon fluorolog3 spectrofluorometer. The electrochemical study, i.e., cyclic voltammetry, was carried out by Gamry ref. 3000 Potentiostat/Galvanostat with a three-electrode system with platinum as working electrode, Ag/Ag+ as reference electrode and a platinum wire as counter electrode along with 0.1 M TBHF in acetonitrile which was used as an electrolyte.

3 Results and discussion

3.1 FTIR studies

The FTIR spectra for BSA-PANI and BSA-PANI interacted with HEMs is shown in Fig. 1 with the peak assignments given in Table 1. The nature of the interaction between BSA-PANI and HEMs is understood from FTIR spectra by analysing the shift in bond stretching frequency of BSA-PANI before and after interaction with HEMs. From FTIR spectra, we observed nine prominent peaks, as shown in Table 1. The peak at 3432 cm^{-1} corresponds to N–H stretching vibration in BSA-PANI, peak at 1634 cm^{-1}

corresponds to N=Q=N stretching vibration, peak at 1496 cm^{-1} corresponds to N–B–N stretching vibration. The phenazine-like structure stretching is observed at 1406 cm^{-1} due to the cross-linked polymer chain formed during synthesis. The peaks at 1298 cm^{-1} , 1182 cm^{-1} and 1132 cm^{-1} correspond to (C–N) stretching of secondary aromatic amine, C–H bending of quinoid unit in the BSA-PANI, and for charge portion of the polymer chain of Q=NH⁺–B or B–NH⁺–B. The HSO₄[−]/SO₃[−] group on the sulfonated aromatic ring of dopant is observed at 1020 cm^{-1} , and the remaining peaks below 1000 cm^{-1} are from dopant HSO₄[−] [20–22]. The π electron delocalization in the polymer is rapid by transforming benzenoid and quinoid units through chemical equilibrium. During the synthesis bipolaron is generated in the initial step which is stabilised through interconversion to polaron by electron delocalisation [23]. The FTIR spectra of BSA-PANI resemble the characteristic peaks of PANI. On interaction with HEMs, few characteristic peaks of BSA-PANI show a small shift. The electron-rich moiety i.e., nitrogen (polaron and bipolaron), π electrons of benzenoid and quinoid units of the BSA-PANI interacts with the nitro groups in HEMs which acts as electron-deficient groups or electron-withdrawing groups. From Table 1, the peak at 3432 cm^{-1} which corresponds to N–H stretching, shows a major shift on interaction with HEMs; this shows that the electron-rich nitrogen in the polymer chain interacts with the HEMs.

The peak at 1634 cm^{-1} corresponding to N=Q=N in the BSA-PANI also shows a significant shift on interaction with HEMs confirming the interaction between the π electrons of quinoid unit in the BSA-PANI with the HEMs, which further stabilises the quinoid unit in the polymer chain. The peak at 1298 cm^{-1} corresponds to $\nu(\text{C–N})$ of secondary aromatic amine i.e., the benzenoid unit attached to nitrogen shows a change in vibration peak, which confirms the interaction between nitrogen attached to

Fig. 1 FTIR Spectra of BSA-PANI and BSA-PANI with HEMs

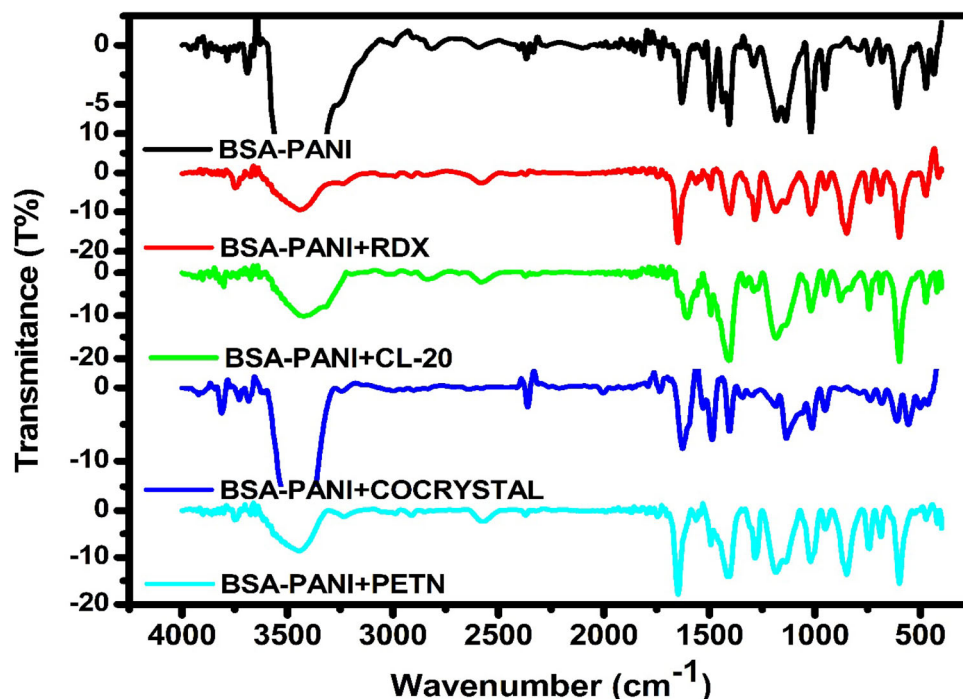


Table 1 FTIR spectral assignment for BSA-PANI and BSA-PANI with HEMs

BSA-PANI in cm^{-1}	BSA-PANI-RDX in cm^{-1}	BSA-PANI-CL-20 in cm^{-1}	BSA-PANI-Cocrystal in cm^{-1}	BSA-PANI-PETN in cm^{-1}	Assignments
3432	3442	3422	3434	3444	N–H stretching of the amine group
1634	1648	1650	1660	1648	N=Q=N Quinoid (Q) unit stretching
1496	1494	1494	1496	1494	N–B–N Benzenoid (B) unit stretching
1406	1402	1406	1406	1414	Phenazine ring stretching
1298	1288	1290	1296	1286	$\nu(\text{C–N})$ of secondary aromatic amine
1182	1186	1184	1182	1184	N=Q=N C–H bending
1138	1138	1142	1138	1138	Q=NH ⁺ –B or B–NH ⁺ –B
610	600	600	606	600	HSO ₄ ⁻ , SO ₄ ²⁻
1020	1020	1020	1016	1020	HSO ₄ ⁻ /SO ₃ ⁻ group on a sulfonated aromatic ring

the benzenoid unit with the nitro group of the HEMs. From Table 1, it is clear that PETN shows notable shifts in the vibration peak, confirming more prominent interaction between the BSA-PANI and the nitro group of PETN when compared to other quenchers. In PETN, the nitro group is attached to the open-chain compared to the nitro group attached to caged HEMs viz., CL-20 and Cocystal shows more accessibility for interaction. The peaks at 1020 cm^{-1}

and below 1000 cm^{-1} form dopant HSO₃⁻¹ do not show any change in frequency on interaction with HEMs confirms there is no destabilisation for dopants attached to the PANI on interaction with HEMs. Further, the peak intensity at 3600 cm^{-1} to 3400 cm^{-1} confirms the secondary interaction between N–H of the BSA-PANI and the HEMs. The other changes in intensity is due to effective charge influenced by the surrounding atoms, which also

confirms the interaction between BSA-PANI and the HEMs. From FTIR spectra, shifts in vibration confirm the formation of a charge-transfer complex between BSA-PANI and HEMs. Further interaction between polymer and HEMs is reported by employing Resonance Raman Spectroscopy (RRS).

3.2 Resonance Raman spectroscopy

In the present paper, the Resonance Raman Spectral (RRS) study is important because it helps to understand the sensitive mechanistic study of the interaction between BSA-PANI and HEMs. From RRS, sensitive C–C vibrations in the polymer chain are studied and used to investigate the structure, electronic properties, and intermediate formed. From literature, the RRS of PANI hydrochloride films and other doped PANI, including BSA-doped along with its base forms, with different laser wavelengths with different laser powers observed various vibrations of the polymer chain. It was observed that at lower laser power at 638 nm laser wavelength, the functionalized PANI shows several peaks for benzenoid, quinoid unit vibrations, phenazine like cross-linkage vibrations, polaron vibrations or radical segment vibrations with other vibrations in the polymer chain [24]. While employing higher laser power caution is taken so that the polymer chain is not damaged through deprotonation. On using higher laser power, only two peaks (1574 cm^{-1} and

1324 cm^{-1}) are shown in Fig. 2 and tabulated in Table 2) were observed due to a change in polarizability ellipsoid during irradiation. These two bonds stretching vibrations are important in the interaction study. The peak at 1574 cm^{-1} is assigned for C=C stretching vibrations of the semiquinoid unit, and the peak at 1324 cm^{-1} is assigned for delocalised polaronic peak or C~N⁺ stretching vibrations of semi quinoid unit. When BSA-PANI interacts with HEMs, these two peaks show a prominent shift indicating interaction with polaron and semiquinoid units. In the RRS, the polaron peak at 1324 cm^{-1} is important and this vibration is FTIR inactive [25, 26]. From Fig. 2, it is clear that PETN interacts with BSA-PANI to a greater extent than other HEMs. The four nitro groups (nitro ester) in PETN are attached to the open-chain has better interactions at these positions. Compared to other HEMs with cage structures with a higher number of nitro groups which are non-accessible to interact with BSA-PANI. The nitrogen groups in PETN freely move and arrange themselves to a structure with higher interaction with the electron-donating polaron unit in the BSA-PANI, showing a more significant shift in peak than other HEMs.

The FTIR and RRS results revealed a strong electrostatic interaction between the BSA-PANI and the HEMs. The FTIR spectrum shows the interaction between the nitrogen of BSA-PANI with the nitro groups of HEMs through a slight shift in N–H

Fig. 2 Resonance Raman Spectra of BSA-PANI and BSA-PANI with HEMs

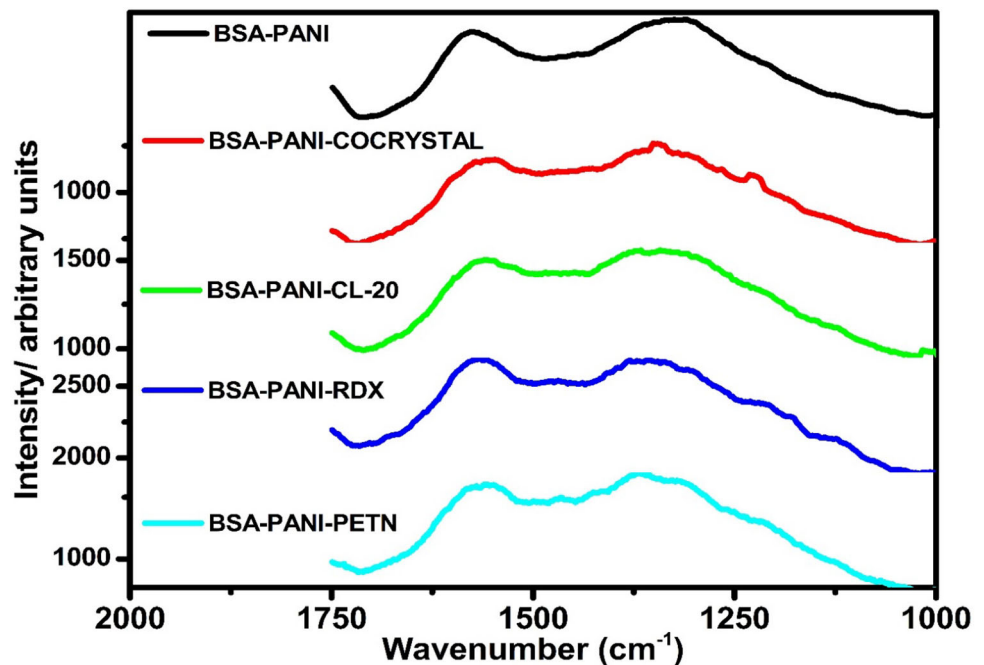


Table 2 Resonance Raman spectral assignment for BSA-PANI and BSA-PANI with HEMs

BSA-PANI in cm^{-1}	BSA-PANI-RDX in cm^{-1}	BSA-PANI-CL-20 in cm^{-1}	BSA-PANI-Cocrystal in cm^{-1}	BSA-PANI-PETN in cm^{-1}	Assignments
1574	1546	1560	1566	1556	C=C stretching vibrations of the semiquinoid unit
1324	1342	1342	1354	1367	C~N ⁺ stretching vibrations of Semi quinoid unit

stretching and also N=Q=N interaction with HEMs. The RRS confirms the interaction between C~N⁺, i.e., polaron in the polymer chain, which is not observed in FTIR.

3.3 UV–Vis spectroscopy

Two distinct peaks at 336 and 562 nm are observed on the UV–Vis spectra for BSA-PANI and are shown in Fig. 3. The peak at 336 nm is due to π - π^* transition of benzenoid and quinoid units of BSA-PANI, while the broad peak near 562 nm is assigned to n - π^* transition of polaron or nonbonding electrons in the polymer chain [27, 28]. At lower wavelengths, the absorbance due to π - π^* transition shows a change in intensity on interaction with HEMs corresponding to the static interaction mode [29] and at higher wavelength, BSA-PANI with HEMs shows the n - π^* transition in the polymer with a slight decrease in

absorbance and a slight shift in wavelength, suggesting the formation of a possible exciplex complex between BSA-PANI to HEMs. The UV–Vis absorption results support the possibility of charge transfer from the BSA-PANI to the energy acceptor HEMs.

3.4 Field-emission scanning electron microscopy (FESEM)

The FESEM images of BSA-PANI and BSA-PANI-HEMs are shown in Fig. 4. The micrographs show polymer aggregation forming a globular structure with a large surface area. Globular structures possess high surface area and are suitable to act as materials optical devices for sensing applications [30]. On interaction with HEMs, polymer morphology does not show significant change showing disorganized structure along with the broken globule-like structures.

Fig. 3 UV–Vis Spectra of BSA-PANI and BSA-PANI with HEMs

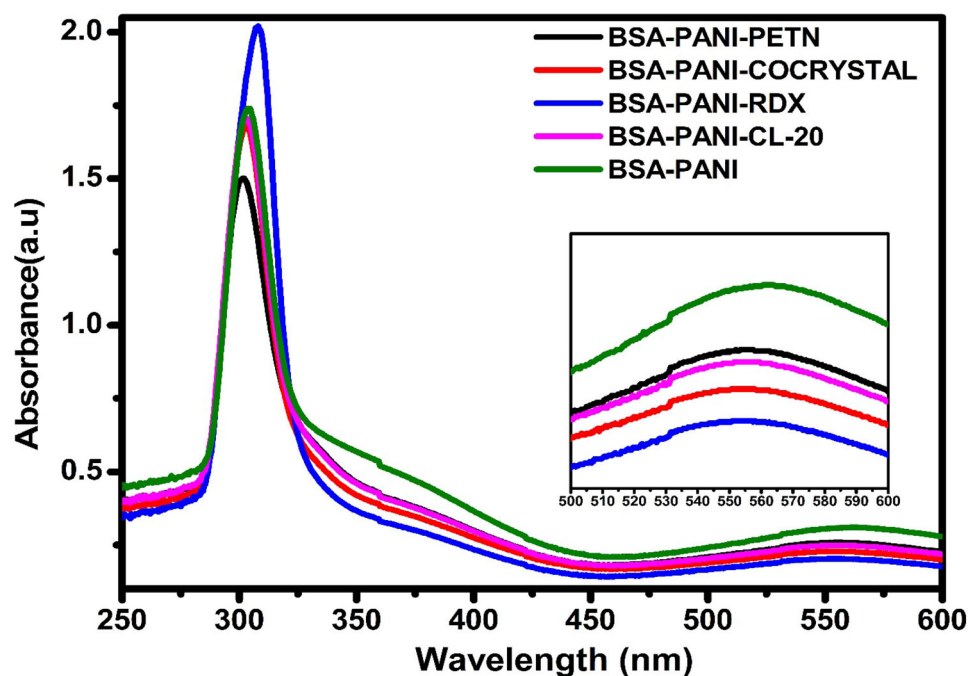
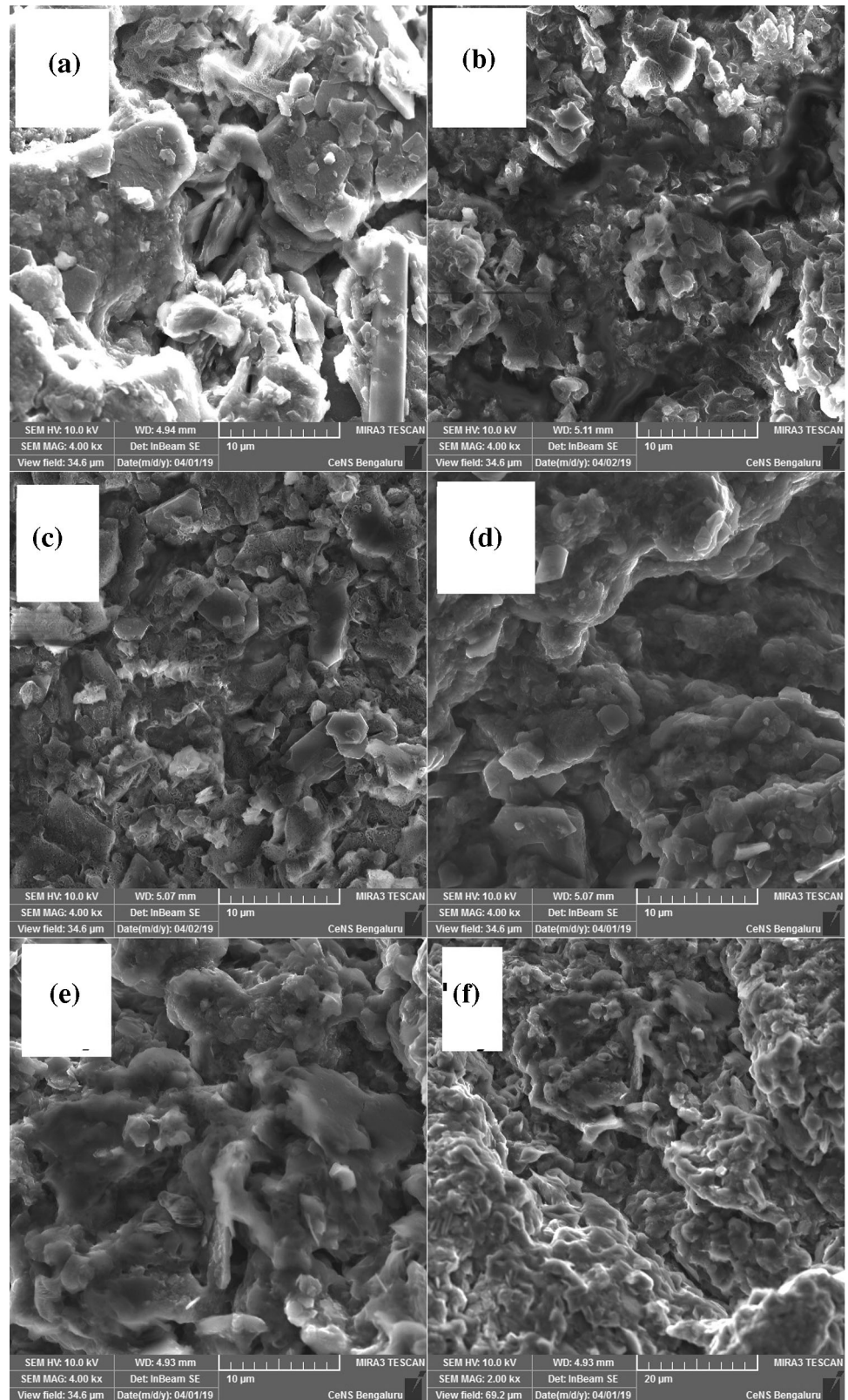


Fig. 4 FESEM images of BSA-PANI (a), BSA-PANI-PETN (b), BSA-PANI-RDX (c), BSA-PANI-CL-20 (d), BSA-PANI-COCRYSTAL (e) & (f)



3.5 Fluorescence study

In the present study, fluorescence quenching experiments are performed using BSA-PANI as fluorophore and HEMs as quenchers in DMF. From fluorescence spectra efficiency of quenchers and the Limit of Detection (LOD) are calculated. The quenching results are shown in Fig. 5 for PETN, CL-20, RDX, and CL-20: RDX Cocystal.

The fluorescence experiments were carried out using 100 ppm BSA-PANI solution in DMF as solvent, which acts as fluorophore in a quartz cell by keeping BSA-PANI concentration constant and varying the concentration of HEMs. The fluorescence emission spectra are recorded on exciting the fluorophore at λ_{max} 352 nm to get the highest intensity peak at 434 nm. Upon gradual addition of quenchers, efficient quenching of the fluorescence intensity was observed. The Stern–Volmer (S–V) plots give quenching efficiency of HEMs and are shown in Fig. 6. On addition of HEMs to BSA-PANI in DMF, fluorescence emission of BSA-PANI is quenched with shift in emission frequency (PETN) are observed. It was observed that CL-20 and Cocystal could quench the fluorescence of BSA-PANI only upto a certain concentration, further addition of CL-20 and Cocystal had no effect on the fluorescence emission of BSA-PANI. The CL-20 and Cocystal are large

caged HEMs in which the nitro groups are attached at different positions of the cage structure, as these nitro groups are inaccessible to interact with BSA-PANI; hence they quench the fluorescence emission of the fluorophore to a lesser extent. Whereas PETN shows quenching to a greater extent even at higher concentrations, along with a shift in maximum emission peak intensity. This is due to the formation of exciplex, which stabilises the excited state [31]. RDX also shows good quenching of fluorescence emission of BSA-PANI without any shift in the maximum emission peak intensity.

It is also interesting to note that as the concentration of HEMs increases, the emission peak shows three peaks at 410 nm, 434 nm and 454 nm along with an additional peak at 394 nm. The peak at 410 nm and 454 nm is due to undoped forms of the reduced and oxidized entity [32]. The main peak at 434 nm is due to π – π^* transition of the doped oxidized form of BSA-PANI and the peak at 394 nm is due to solvent impurities [33, 34]. The fluorescence in the BSA-PANI is due to the presence of π – π^* transition of the benzenoid unit present in the polymer chain and the quinoid unit in the polymer chain quenches the fluorophore to a considerable extent [35]. The HEMs on interaction with BSA-PANI causes fluorescence intensity changes by the interaction of electron-withdrawing nitro group of HEMs with

Fig. 5 Fluorescence Spectra of BSA-PANI with HEMs

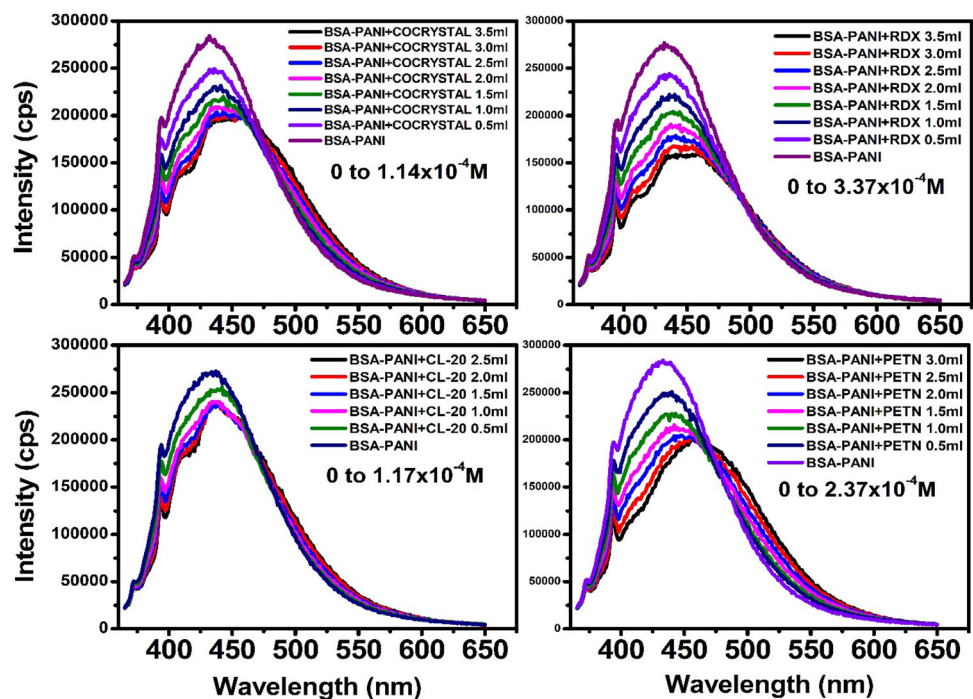
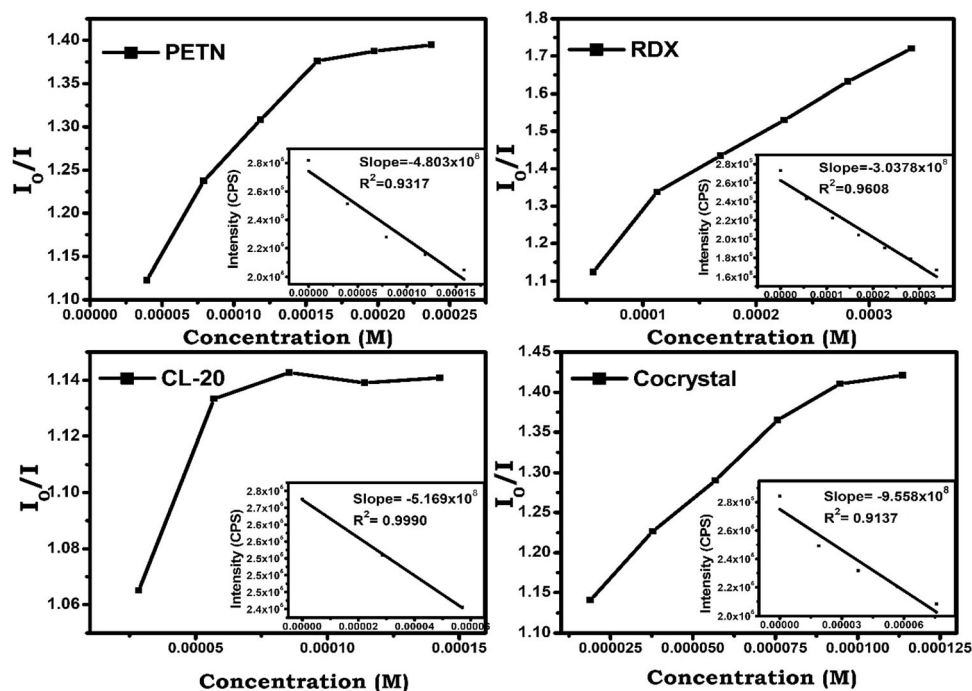


Fig. 6 Stern–Volmer Plots inserted with LOD plots for BSA-PANI with HEMs



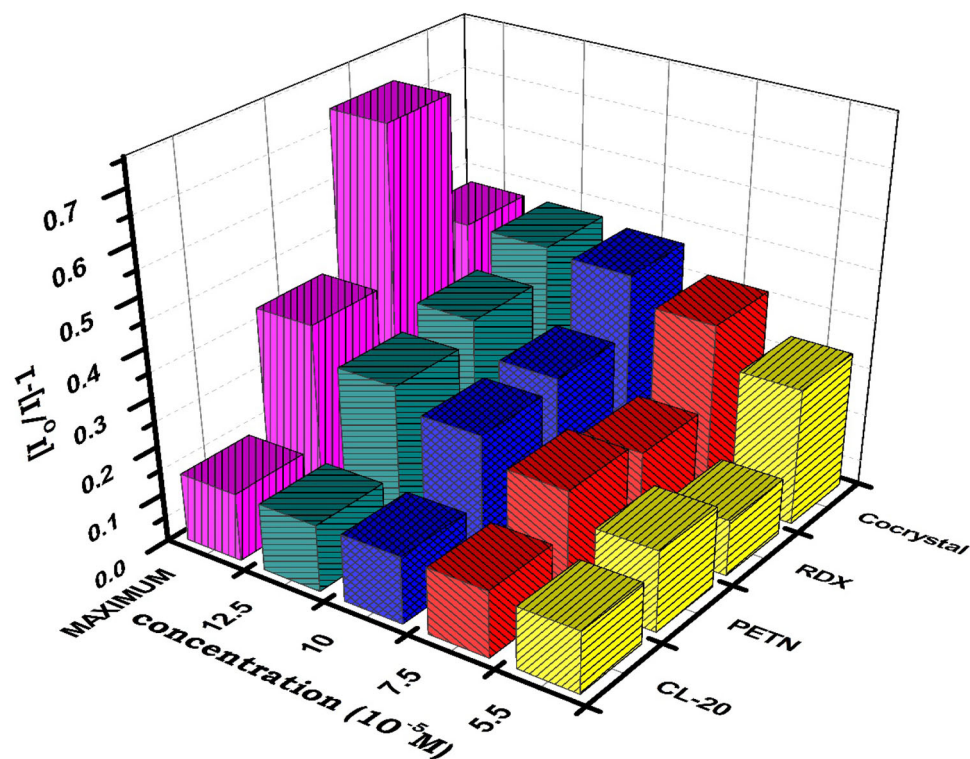
electron-rich π bonded centres, localised and delocalised polarons of the amine group of BSA-PANI.

A Stern–Volmer (S–V) plot is plotted by taking I_0/I Vs the concentration of quencher. The Stern–Volmer constant (K_{sv}) can be determined by calculating the slope of the S–V plots (Fig. 6), which provides an information of the quenching efficiency and the mechanism of quenching [36]. It is observed from the S–V plots that at a lower concentration of HEMs, all the plots are linear. While at higher concentration of the HEMs viz. CL-20 and Cocrysal, the quenching efficiency becomes saturated, leading to deviation from linearity, while for PETN and RDX, the plot remains linear, indicating amplified quenching process as shown in Fig. 6. From the slope of the S–V plots for PETN and RDX, quenching constants were found to be $2.103 \times 10^3 \text{ M}^{-1}$ (PETN) and $2.010 \times 10^3 \text{ M}^{-1}$ (RDX), whereas the linear part of CL-20 shows K_{sv} constant $2.394 \times 10^3 \text{ M}^{-1}$ (CL-20) and $3.541 \times 10^3 \text{ M}^{-1}$ (Cocrysal). From the S–V plots, it is observed that quenching constant is higher for Cocrysal as compared to other HEMs at lower concentration. The LOD for HEMs was obtained from the plot of fluorescence intensity Vs their concentration as shown in Fig. 6. LOD for HEMs then calculated using the formula $3S/K$, where S is the standard deviation and the K is slope [30, 37]. These results demonstrate that BSA-PANI can function as a highly

sensitive and selective detector towards Cocrysal at a lower concentration (which has a higher number of NO_2 groups) when compared with other HEMs like CL-20, RDX, PETN. However, all HEMs show remarkable sensing with the fluorophore. Using the above formula, the LOD for Cocrysal was found to be $1.876 \times 10^{-5} \text{ M}$, and LOD for CL-20, RDX, PETN was found to be $3.191 \times 10^{-5} \text{ M}$, $5.904 \times 10^{-5} \text{ M}$, $3.734 \times 10^{-5} \text{ M}$. The highest quenching of HEMs is obtained for RDX compared to other HEMs and this is observed from Fig. 7.

The NO_2 group plays a vital role in fluorescence quenching, which withdraws electron from the polymer chain. The Cocrysal shows higher quenching constant because of more number of NO_2 groups compared to other HEMs. At higher concentrations of HEMs, the strained structure in CL-20 and Cocrysal limits the quenching; thus, there is no quenching observed after a certain concentration but for RDX and PETN shows quenching even at higher concentration are shown in Fig. 7. Here the accessibility of the nitro group plays an essential role in quenching. It may be understood that the RDX possess a planar structure with a moderately higher charge on the nitro group when compared with other strained HEMs used in the study, and thus has more accessibility for interaction.

Fig. 7 Quenching efficiency of different HEMs at different concentration



Absorbance spectra of HEMs also show quencher behaviour by overlapping with the normalized fluorescence spectra of BSA-PANI, as shown in Fig. 8. Figure 8 shows no overlap between emission spectra of BSA-PANI and absorption spectra of HEMs, indicating that the fluorescence emission energy is insufficient to absorb and excite electrons in the quencher, thereby indicating the absence of the inner filter effect. To understand the selectivity of different HEMs, the quenching mechanism was investigated;

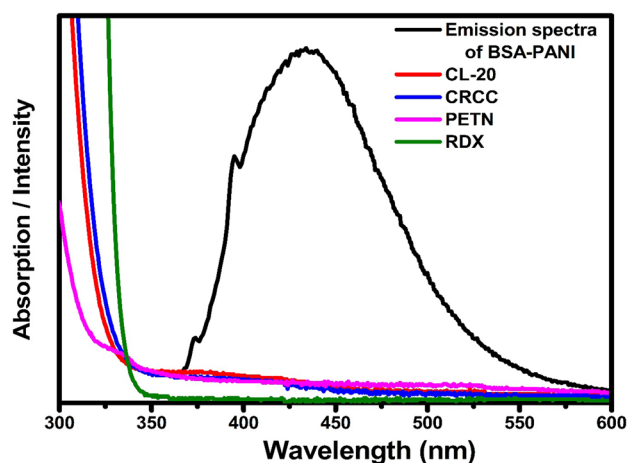


Fig. 8 Absorption spectra of HEMs and emission spectra of BSA-PANI

the quenching phenomenon and fluorescence may be explained by electron transfer of donor–acceptor groups through the interaction of electron-rich BSA-PANI with electron-deficient analytes (HEMs). The electron transfer takes place in the ground state by forming a complex or in the excited state by collision. Using molecular orbital theory, the electron transfer is understood. The electron transfer from lowest unoccupied molecular orbital (LUMO) of the excited fluorophore to LUMO of HEMs occurs only if the LUMO of HEMs lie below LUMO of the fluorophore [38]. Therefore, the electron-deficient analyte stabilises the electron transfer from the HOMO to LUMO of BSA-PANI, which is higher than the LUMO of HEMs, making it thermodynamically favourable. Further understanding on the mechanism is obtained from electrochemical studies i.e. cyclic voltammetry studies discussed in the next section.

The linear plot for PETN and RDX suggests quenching occurs through single mechanism either static or dynamic. The interaction between nitro group of these with forming electron donor–acceptor complex was confirmed by Resonance Raman and FTIR studies as discussed earlier. Moreover, CL-20 and Cocrysal show nonlinear plots suggesting multiple mechanisms. As there is no overlap of the

absorption spectra of quencher and emission spectra of fluorophore possible FRET (Fluorescence Resonance Energy Transfer) mechanism is not observed. It is understood from these S–V plots that the mechanism of fluorescence is through PET (Photoinduced Electron Transfer) as the excited electron transfer takes place through the thermodynamically favourable route (LUMO of the fluorophore to LUMO of quencher) non radiatively shown in Fig. 9 [39].

3.6 Cyclic voltammetry

Numerous electrochemical techniques are available for the detection of HEMs with various redox-active reagents in the accessible potential range possessing good sensitivity, selectivity and suitable concentration range [40–42]. The most commonly used electrochemical techniques are stripping voltammetry, square wave voltammetry and cyclic voltammetry. Stripping voltammetry is a preconcentration technique with lowest limit of detection among other electrochemical techniques. Amongst all the electrochemical techniques, the cyclic voltammetry technique, which distinguishes the oxidation and reduction in the single run plays a key role in understanding such processes. Cyclic voltammetry is one such important electrochemical technique wherein one will observe both oxidation and reduction process, and the technique is highly sensitive and selective. Ramanavicius et al. gave a critical review on the use of conducting polymer as electrochromic sensors in cyclic voltammetric study for selective and sensitive sensing of heavy metal ions, various gases, humidity, chemical and biochemical compounds [43, 44].

In our study, we employed BSA-PANI for cyclic voltammetry for the detection of HEMs (RDX, CL-20, and Cocystal). The sensitivity and selectivity of these analytes towards BSA-PANI are understood through the changes observed in current intensity and shift in

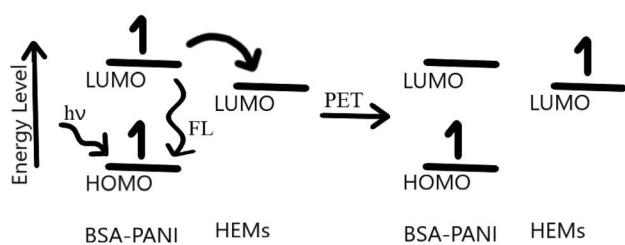


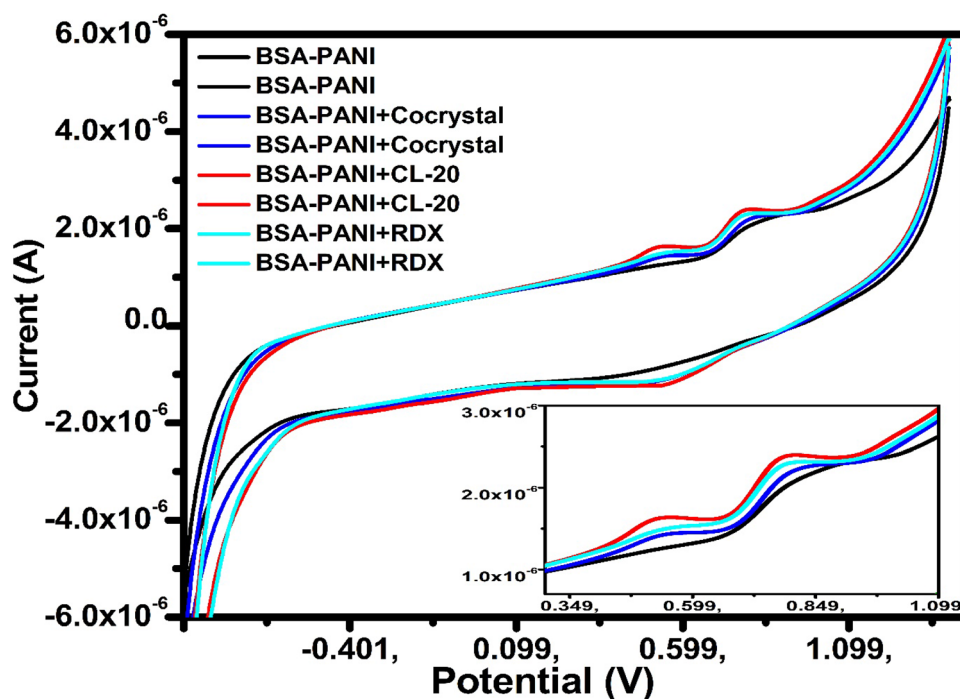
Fig. 9 Fluorescence quenching mechanism

the CV traces oxidation potential peak positions. From the literature, the reduction potential peak intensities are studied for detection of HEMs by studying the nitro groups reduction process on applying the potential [41, 42]. HEMs on interaction with the BSA-PANI with multiple stable oxidation forms (pernigraniline, emeraldine and leucoemeraldine) lead to a shift in the applied potential. BSA-PANI possess a partially oxidised form, emeraldine (with three moieties of benzenoid units possessing amine linkage and one moiety of quinoid unit, with imine linkages), which further fully oxidises to pernigraniline (equal numbers of benzenoid units and Quinoid units) and these transitions are observed at two different oxidation potentials viz 0.7 V and above 1.159 V respectively. Similarly, the emeraldine base (a partially reduced form with three benzenoids and one quinoid unit) reduces fully to leucoemeraldine (only benzenoid units with amine linkages).

The CV studies are conducted in the presence of the electrolyte solution, i.e., Tetrabutyl ammonium hexafluorophosphates (TBHF) in acetonitrile solvent with an applied potential range from -0.9 to $+1.4$ V with a scan rate of 0.05 V/s up to 20 cycles to stabilize the electrochemical activity of BSA-PANI and BSA-PANI with HEMs [45]. Further, it is observed that the morphology plays an important role in electrochemically accessible sites and the diffusion path, which impact the electrochemical behaviour of polyaniline/doped polyaniline giving rise to different shapes in the cyclic voltammograms and at higher scan rate possess better retention [46, 47].

The overlap of BSA-PANI and BSA-PANI with HEMs, CV shows a variation in oxidation potential and reduction potential before and after the interaction. The CV trace in Fig. 10 shows a single peak at (0.78 V) for merged bipolaronic and polaronic peaks due to rapid transitions between polaron to bipolaron during the oxidation cycle in the BSA-PANI, but in the presence of HEMs, the two peaks are separately seen in CV. This observation indicates the conversion of polaron to bipolaron is stabilised by electron-deficient nitro groups of HEMs by withdrawing the electron from the BSA-PANI chain. The reverse scan in the reduction zone also shows this behaviour, thereby indicating that partially and the fully reduced forms (i.e., emeraldine base and pernigraniline) possess very close oxidation and reduction potentials. It may with caution be mentioned here

Fig. 10 Cyclic voltammeter curve of BSA-PANI and BSA-PANI with HEMs



that the doped BSA functionality plays a critical role in electrochemical treatment, reducing the oxidation and reduction potentials. Figure 10 shows the CV trace of BSA-PANI and BSA-PANI-HEMs; it is observed that oxidation and reduction peaks are shifted to a slightly higher or lower potential than that of BSA-PANI (BSA-PANI:0.832 V, BSA-PANI-RDX:0.805 V, BSA-PANI-Cocrysal: 0.786 V and BSA-PANI-CL-20:0.778 V) with a significant change in the current (BSA-PANI: 2.15×10^{-6} A to BSA-PANI-CL-20: 2.362×10^{-6} A). CL-20 stabilises the polaron and bipolaron units in the polymer chain at particular potentials interacting the nitro groups of CL-20 with BSA-PANI at a lower concentration than other HEMs with slightly increased current peak, shows the interaction of BSA-PANI with HEMs influences the electrochemical properties of BSA-PANI.

4 Conclusions

In this study, BSA-PANI is used as a fluorophore to understand the interaction between the BSA-PANI and commercial HEMs (RDX, PETN, CL-20, and CL-20: RDX Cocrysal). The BSA-PANI shows higher sensitivity towards RDX. FTIR and Raman spectra characterisation studies show the interactions between BSA-PANI and HEMs. Electrochemical

detection studies show that emeraldine form of BSA-PANI is sensitive towards HEMs with stabilisation of polaron and bipolarons on interaction of BSA-PANI with HEMs. Spectral and electrochemical studies help in understanding the number and arrangement of NO_2 groups in HEMs involved in the interaction. The overall study has shown BSA-PANI can act as a potential fluorophore for detection of highly important HEMs through fluorescence quenching method and interesting details of the chemistry between the fluorophore and the quencher are neatly presented in this paper through spectroscopic and electrochemical studies approach.

Acknowledgements

The authors acknowledge and thank Prof. G. U. Kulkarni, the former Director of Centre for Nano and Soft Matter (CeNS) for providing the facility to work in the centre. The authors, S A Ture and V B Patil, expresses their thanks to M/s Premier Explosive Limited for their Financial support (H/A: 4254), the corresponding author expresses his thanks to UGC, New Delhi for the BSR faculty fellowship [F.4-5(11)/2019(BSR)]. We also thank the Spanish Government [RTI2018-100910-B-C41 (MCUI/AEI/FEDER, UE)]

and Generalitat Valenciana (PROMETEO2018/024) for their support.

Declarations

Conflict of interest There are no conflicts of interest to declare.

References

- C. Zhang, X. Pan, S. Cheng, A. Xie, W. Dong, J. Lumin. **233**, 117871 (2021)
- S. Shanmugaraju, S.A. Joshi, P.S. Mukherjee, J. Mater. Chem. **21**, 9130–9138 (2011)
- D.S. Moore, Rev. Sci. Instrum. **75**, 2499–2512 (2004)
- A.L. Lehnert, K.J. Kearfott, Nucl. Technol. **172**, 325–334 (2010)
- J.-S. Yang, T.M. Swager, J. Am. Chem. Soc. **120**, 5321–5322 (1998)
- J.-S. Yang, T.M. Swager, J. Am. Chem. Soc. **120**, 11864–11873 (1998)
- S.W. Thomas, G.D. Joly, T.M. Swager, Chem. Rev. **107**, 1339–1386 (2007)
- H. Nie, H. Ma, M. Zhang, Y. Zhong, Talanta **144**, 1111–1115 (2015)
- H.P. Martínez, C.D. Grant, J.G. Reynolds, W.C. Trogler, J. Mater. Chem. **22**, 2908–2914 (2012)
- R. Martínez-Máñez, F. Sancenón, Chem. Rev. **103**, 4419–4476 (2003)
- L.A. Juárez, A.M. Costero, F. Sancenón, R. Martínez-Máñez, M. Parra, P. Gaviña, Chem. Eur. J. **21**, 8720–8722 (2015)
- R. Martínez-Máñez, F. Sancenón, J. Fluoresc. **15**, 267–285 (2005)
- L. Venkatappa, S.A. Ture, C.V. Yelamaggad, V.N.N. Sundaram, R. Martínez-Máñez, V. Abbaraju, ChemistrySelect **5**, 6321–6330 (2020)
- V.B. Patil, S.A. Ture, C.V. Yelamaggad, M.N. Nadagouda, A. Venkataraman, Z. Anorg. Allg. Chem. **647**, 331–340 (2021)
- M. Rong, L. Lin, X. Song, T. Zhao, Y. Zhong, J. Yan, Y. Wang, Xi. Chen, Anal. Chem. **87**, 1288–1296 (2015)
- J. Venkata Viswanath, K.J. Venugopal, N.V. Srinivasa Rao, A. Venkataraman, Def. Technol. **12**, 401–418 (2016)
- J.V. Viswanath, B. Shanigaram, P. Vijayadarshan, T.V. Chowadary, A. Gupta, K. Bhanuprakash, S.R. Niranjana, A. Venkataraman, Propellants Explos. Pyrotech. **44**, 1570–1582 (2019)
- A.G. MacDiarmid, J.C. Chiang, M. Halpern, W.S. Huang, S.L. Mu, L.D. Nanaxakkara, S.W. Wu, S.I. Yaniger, Mol. Cryst. Liq. Cryst. **121**, 173–180 (1985)
- A.G. MacDiarmid, J.C. Chiang, A.F. Richter, N.L.D. Somasiri, A.J. Epstein, in *Conducting polymers*. ed. by L. Alcácer (Springer, Dordrecht, 1987), pp. 105–120
- Z. Morávková, P. Bober, Int. J. Polym. Sci. **2018**, 1797216 (2018)
- J.E. Pereira da Silva, M.L. Temperini, S.I. Córdoba de Torresi, J. Braz. Chem. Soc. **16**, 322–327 (2005)
- M. Trchová, J. Stejskal, Pure Appl. Chem. **83**, 1803 (2011)
- J. Scotto, M.I. Florit, D. Posadas, Electrochim. Acta **268**, 187–194 (2018)
- S.A. Ture, V.B. Patil, C.V. Yelamaggad, R. Martínez-Máñez, V. Abbaraju, J. Appl. Polym. Sci. **138**, 50776 (2021)
- G.M. do Nascimento, M.R. Temperini, J. Raman Spectrosc. **39**, 772–778 (2008)
- M. Jain, S. Annapoorni, Synth. Met. **160**, 1727–1732 (2010)
- R. Borah, S. Banerjee, A. Kumar, Synth. Met. **197**, 225–232 (2014)
- D. Kumar, M. Iwamoto, Polym. J. **45**, 160–165 (2013)
- F. Noun, E.A. Jury, R. Naccache, Sensors **21**, 1391 (2021)
- Li. Wenfeng, Ma. Hengchang, L. Ziqiang, RSC Adv. **4**, 39351–39358 (2014)
- S. Pramanik, Z. Hu, X. Zhang, C. Zheng, S. Kelly, J. Li, Chem. Eur. J. **19**, 15964–15971 (2013)
- M. Baibarac, A. Matea, M. Daescu, I. Mercioniu, S. Quillard, J.-Y. Mevellec, S. Lefrant, Sci. Rep. **8**, 9518 (2018)
- C. Albrecht, Anal. Bioanal. Chem. **390**, 1223–1224 (2008)
- S. Chatterjee, S. Basu, N. Ghosh, M. Chakrabarty, Chem. Phys. Lett. **388**, 79–83 (2004)
- J.Y. Shimano, A.G. MacDiarmid, Synth. Met. **123**, 251–262 (2001)
- C.M. Samworth, M. Degli Esposti, G. Lenaz, Eur. J. Biochem. **171**, 81–86 (1988)
- Q. Li, X. Tan, Fu. Lingli, Qu. Liu, W. Tang, Anal. Methods **7**, 614–620 (2015)
- Wu. Xiaofu, H. Hang, H. Li, Y. Chen, H. Tong, L. Wang, Mater. Chem. Front. **1**, 1875–1880 (2017)
- M. Do Nascimento Gustavo, in *Nanofibers*. ed. by A. Kumar (IntechOpen, Rijeka, 2010), pp. 349–366
- J. Wang, G. Liu, Wu. Hong, Y. Lin, Anal. Chim. Acta **610**, 112–118 (2008)
- A. Üzer, Ş. Sağlam, Y. Tekdemir, B. Ustamehmetoğlu, E. Sezer, E. Erçağ, R. Apak, Talanta **115**, 768–778 (2013)
- H. Gurumalles Prabu, M.B. Talawar, T. Mukundan, S.N. Asthana, Combust. Explos. Shock Waves **47**, 87 (2011)
- R. Celiesiute, A. Ramanaviciene, M. Gicevicius, A. Ramanavicius, Crit. Rev. Anal. Chem. **49**, 195–208 (2019)
- A. Kausaite-Minkstimiene, L. Glumbokaite, A. Ramanaviciene, A. Ramanavicius, Microchem. J. **154**, 104665 (2020)
- S.N. Bhadani, M.K. Gupta, S.K. Gupta, J. Appl. Polym. Sci. **49**, 397–403 (1993)

46. A. Eftekhari, L. Li, Y. Yang, J. Power Sources **347**, 86–107 (2017)
47. A. Sumboja, U.M. Tefashe, G. Wittstock, P.S. Lee, Adv. Mater. Interfaces **2**, 1400154 (2015)

Publisher's Note Springer Nature remains neutral with regard to jurisdictional claims in published maps and institutional affiliations.